National Aeronautics and Space Administration

Advances in Structural Analysis Methods for Structural Health Management of NextGen Aerospace Vehicles

Dr. Alex Tessler
NASA Langley Research Center

2011 Annual Technical Meeting
May 10–12, 2011
St. Louis, MO

Outline

- Motivation
- Vehicle Health Management
- Shape-sensing
- Shape-sensing (NASA Dryden)
- Full-field reconstruction (NASA LaRC)
- Collaborations
- Summary

Motivation: Sensing of wing deformations

FBG strain sensing – wing deformation (inverse reconstruction, ill-posed problem)

Conforming antenna on
AEW&C (airborne radar system)

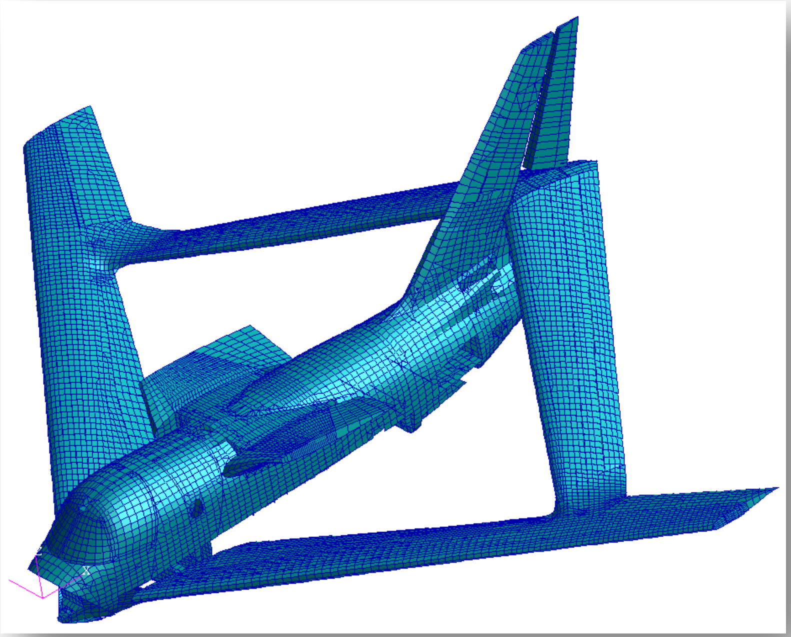

Strain-displacement relations

$$\boldsymbol{\varepsilon}^h = \mathbf{L}\,\mathbf{u}^h \text{ on } \Omega^h$$

Shape sensing: from in-situ strains to deformed shape

Hat-stiffened panel:
full-field solution

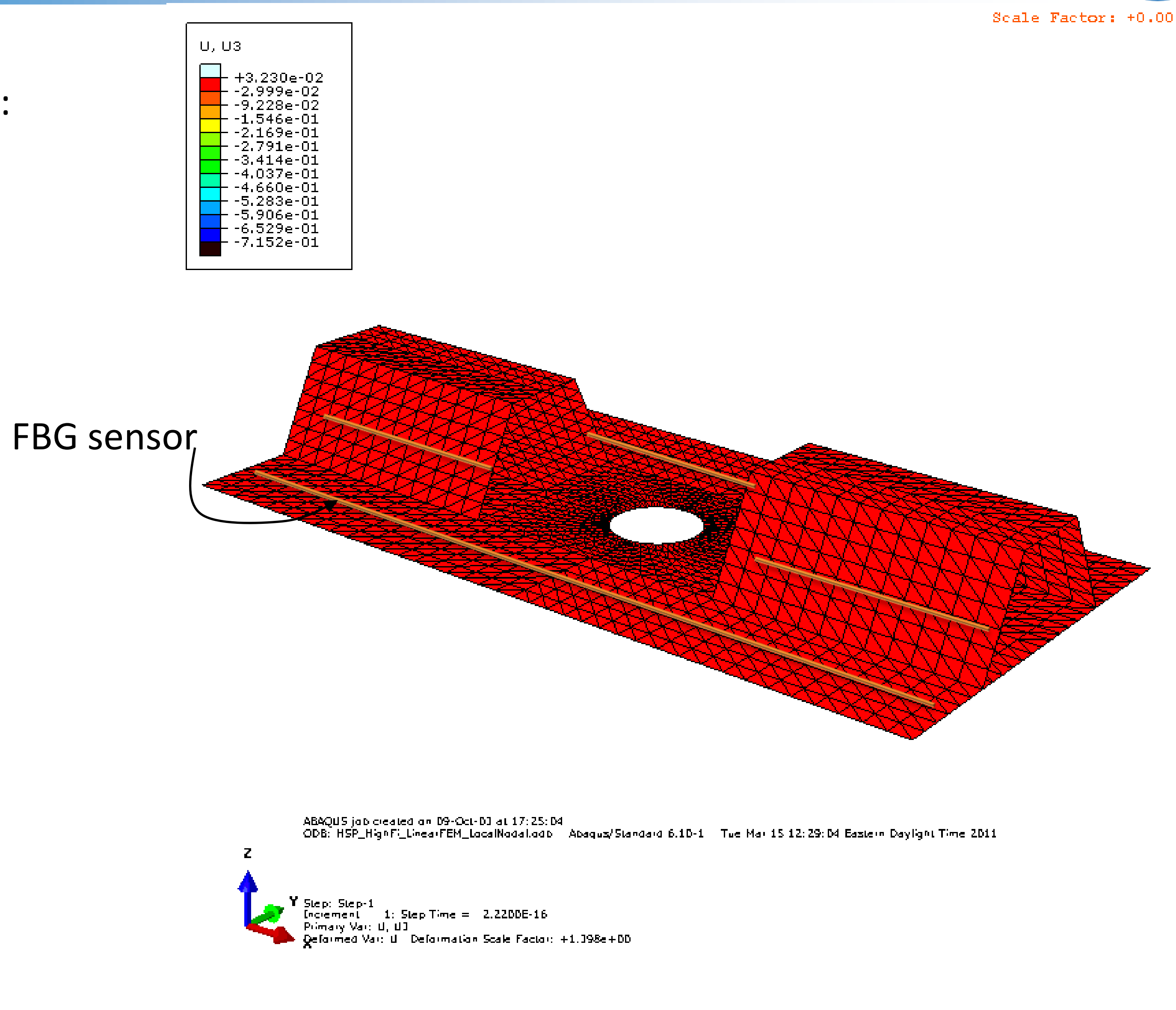

Vehicle Health Management

Objectives

- Affordable, safe and reliable technologies for aeronautic and long-duration space structures
  - Provide real-time vehicle health information via sensors, software and design by monitoring critical structural, propulsion, and thermal protection systems
  - Provide valuable information to adaptive control systems to mitigate accidents due to failure and achieve safe landing
  - Provide detection and localization of impact events on key structural and flight control surfaces
  - Utilize decision-making mechanisms using intelligent reasoning based on safe-outcome probability
  - Maximize performance and service life of vehicle or space structure

Continuous Monitoring and Assessement of Structural Response in Real Time

- Diagnosis and prognosis of structural integrity
  - Deformation
  - Temperature
  - Strains and stresses (internal loads)
  - Damage and failure

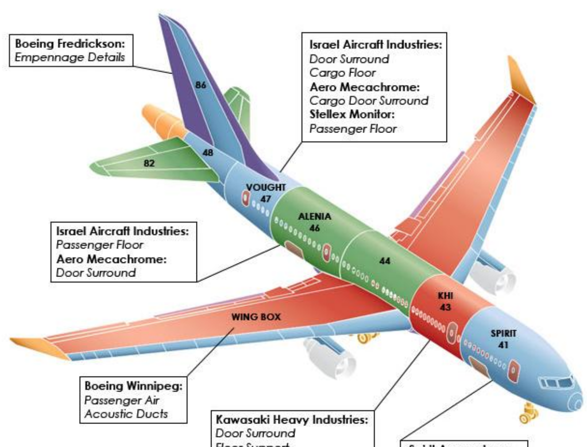

Maximize Performance: Provide Active Structural Control via Shape Sensing

- Helios class of aircraft (solar panel)
  - Control of wing dihedral
- Unmanned Aerial Vehicles (UAV)
- Morphing capability aircraft
  - Shape changes of aircraft wing
- Embedded antenna performance
- Shape control of large space structures
  - Solar sails
  - Membrane antennas

Wing control systems

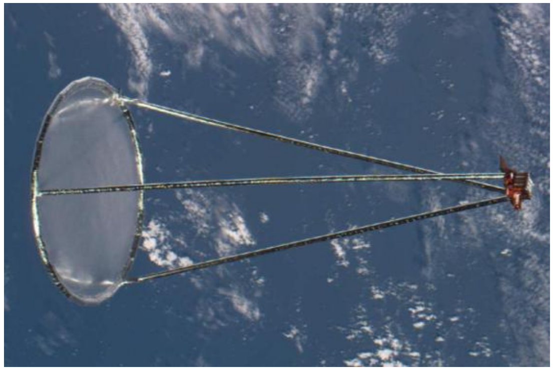

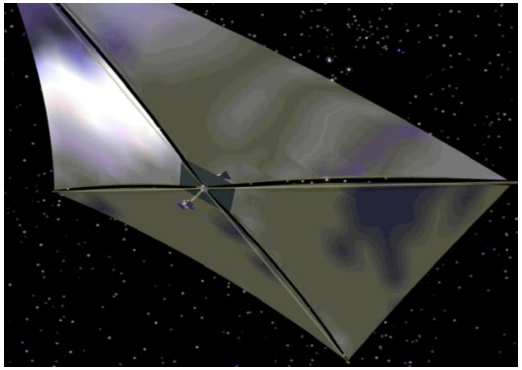

Shape Control of Space Structures

Implementation & enabling capabilities

- Diverse arrays of distributed in-situ sensors
  - Process, communicate, and store massive amounts of SHM data
  - Perform on-board structural analysis based on SHM sensing data
    - Determine deformed shape of structure continuously
    - Perform diagnosis and prognosis of structural integrity
  - Provide information of structural integrity to cockpit displays and remote monitoring locations to enable safe and effective operational vehicle management and mission control
  - Provide valuable information to improve future designs

NASA Dryden Shape-Sensing Analysis

- 1-D integration of classical beam Eqs for cantilevered, non-uniform cross-section beams (no shear deformation)

$$w_{,xx} = \frac{\varepsilon_x^+}{-c(x)} \quad (u_x(x,z) = -z\,w_{,x})$$

$$z \in [c, -c]$$

- Piecewise linear approximation of strain and taper between regularly spaced “nodes” where strains are measured

- Neutral axis is computed from detailed FEM (SPAR code)

- Incorporates cross-sectional geometry of a wing in a beam-type approximation

View from above the left wing
(Optical fiber is glued on top of wing)

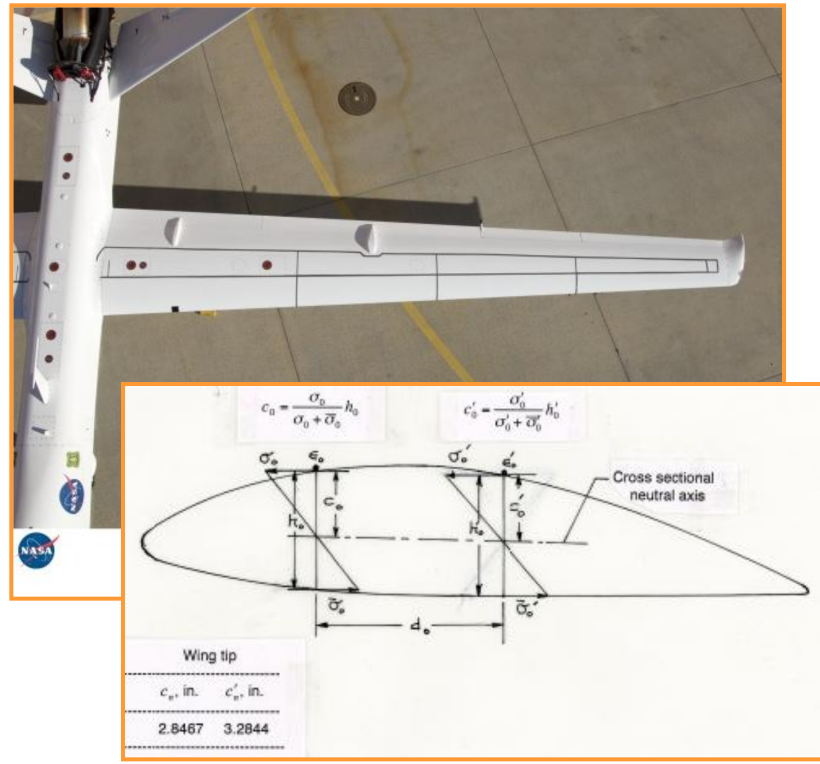

Method for Real-Time Structure Shape-Sensing, U.S. Patent No. 7,520,176, issued April 21, 2009.

NASA Dryden Shape-Sensing Analysis

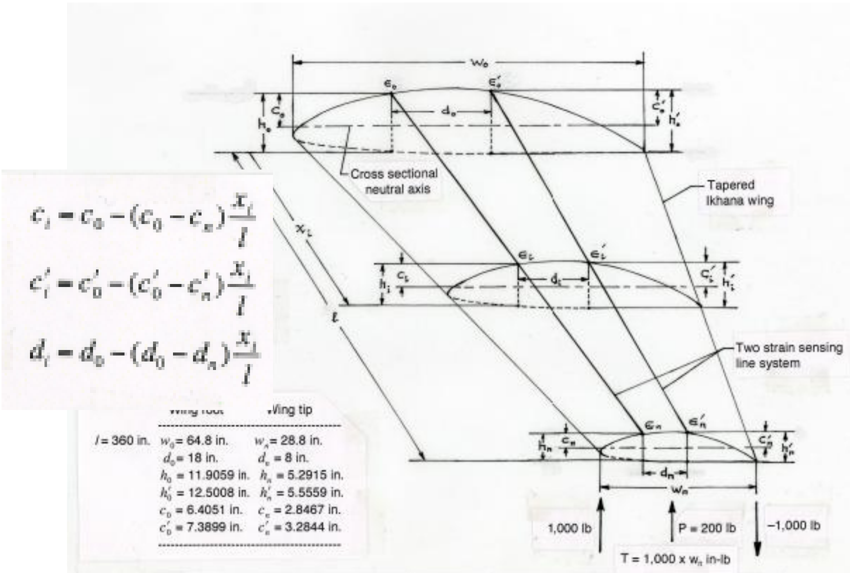

Figure 2. Tapered Ikhana wing installed with two-strain-sensing-line system on upper surface.

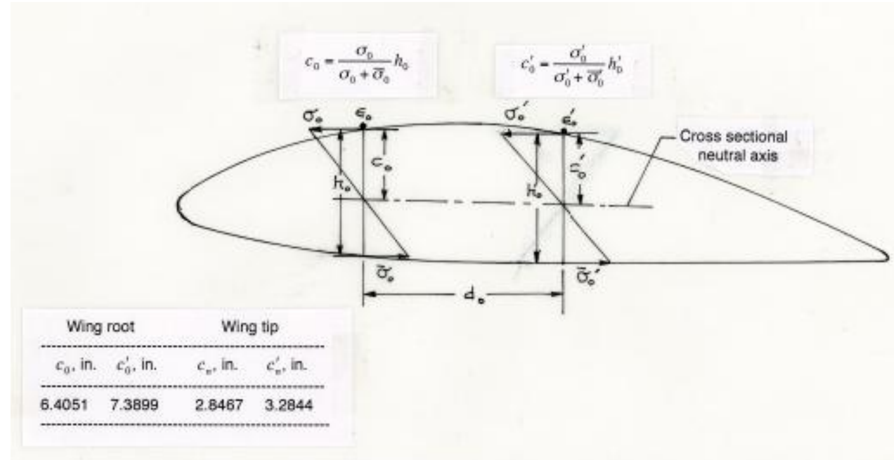

Figure 4. Determination of neutral axis for Ikhana wing root cross section using SPAR bending stress outputs.

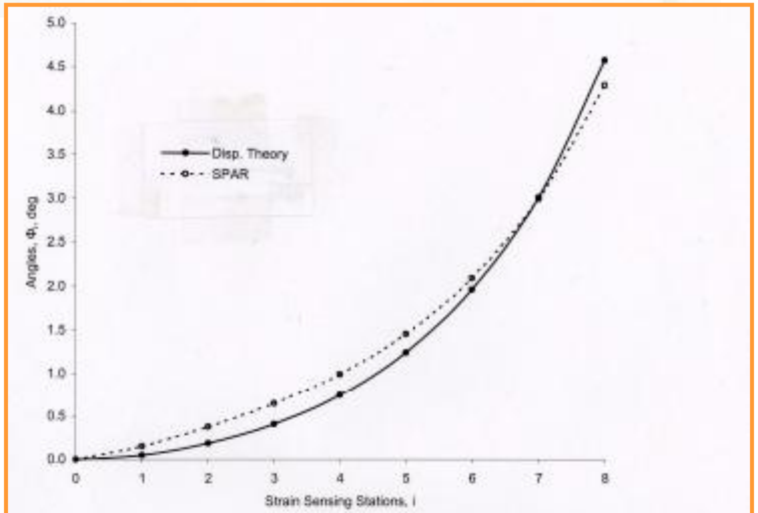

Comparison of Ikhana wing cross sectional twist angles predicted from Ko displacement theory and calculated from SPAR.

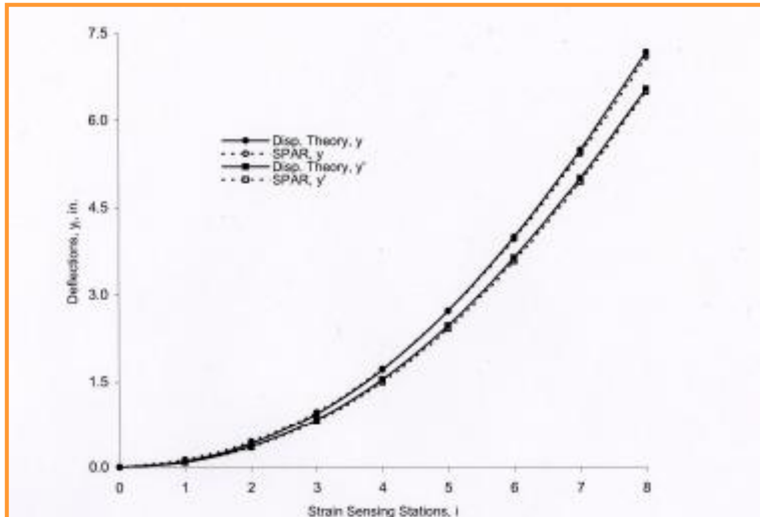

Figure 6. Comparison of Ikhana wing deflections predicted from Ko displacement theory and calculated from SPAR.

NASA LaRC High-Fidelity, Full-Field Inverse FEM

From strains measured at discrete locations, determine full-field continuous displacements, strains, and stresses that represent the measured data with sufficient accuracy

$$\left\{\mathbf{u}, \quad \boldsymbol{\varepsilon}, \quad \boldsymbol{\sigma}, \quad \mathbf{f}(\boldsymbol{\varepsilon},\boldsymbol{\sigma}) = 0 \quad \mathbf{F}_{\mathrm{ext}}\right\}$$

Wing

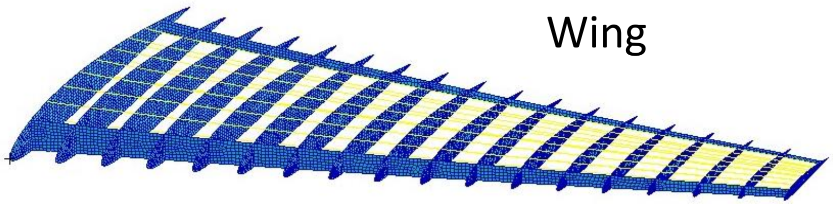

Aircraft

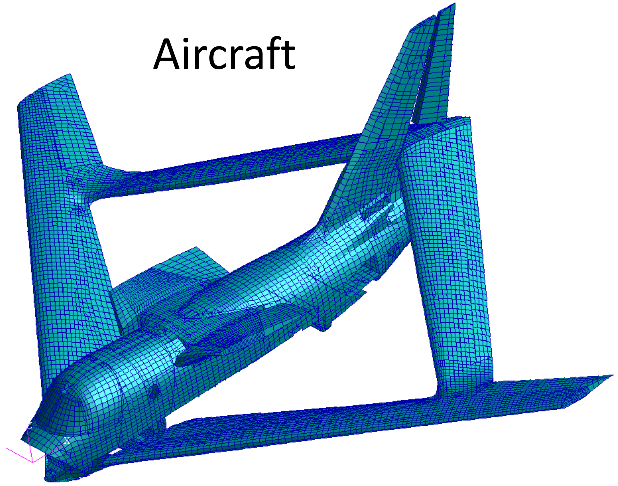

Frame

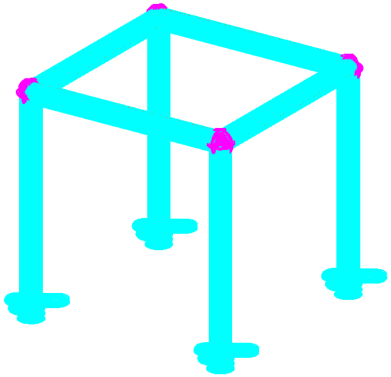

Composite and sandwich structures

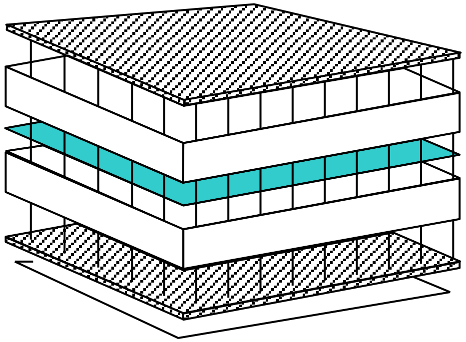

Conceptual Framework of Inverse FEM: Discretized, high-fidelity solution

1. Discretization with iFEM:
   - beam, plate, shell or solid Ω^h
2. Elements defined by a continuous displacement field $\mathbf{u}^h(\mathbf{x})$
3. Strains defined by strain-displacement relations
   $$\boldsymbol{\varepsilon}^h = \mathbf{L}\,\mathbf{u}^h \text{ on } \Omega^h$$
4. Experimental strain-gauge data and iFE strains match up in a least-squares sense
   $$\left\|\Delta\boldsymbol{\varepsilon}\right\|^2 = \left(\boldsymbol{\varepsilon}^h - \boldsymbol{\varepsilon}^{\varepsilon}\right)^2_{xi}$$
5. Displacement B.C.'s prescribed
   $$\mathbf{u} = \bar{\mathbf{u}} \text{ on } \partial\Omega$$
6. Linear algebraic Eqs determine nodal displacements
7. Element-level substitutions yield full-field strains, stresses (internal loads), and failure criteria $\boldsymbol{\sigma}^h = \mathbf{C}\,\boldsymbol{\varepsilon}^h$ on Ω^h

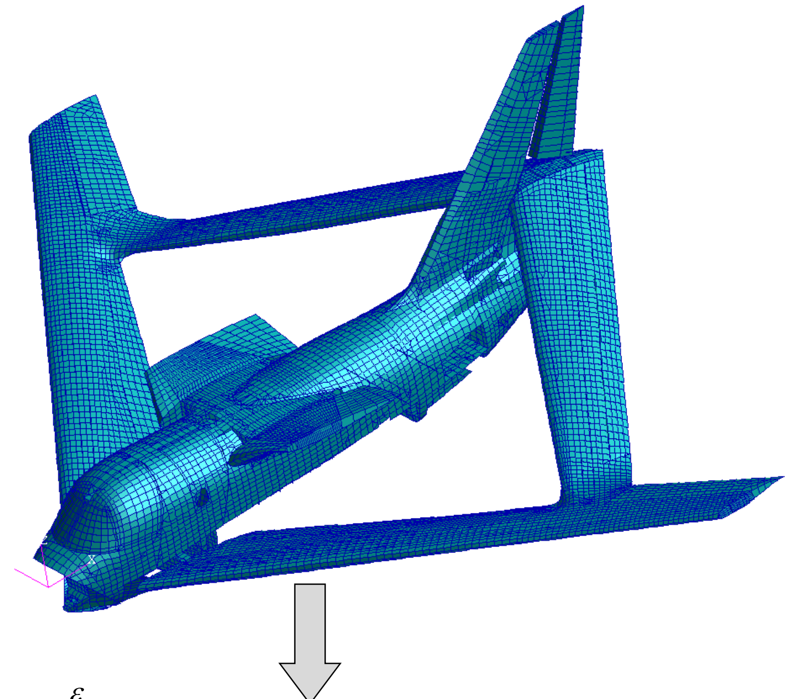

$\boldsymbol{\varepsilon}^{\varepsilon}$

strain at sensor

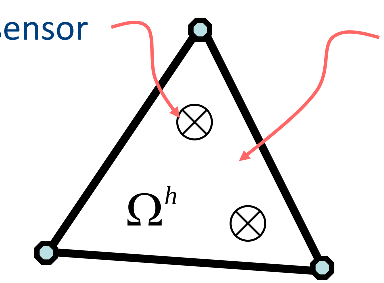

$\mathbf{u}^h = \mathbf{u}^h(\mathbf{x})$

$\boldsymbol{\varepsilon}^h = \mathbf{L}\,\mathbf{u}^h$

$\boldsymbol{\sigma}^h = \mathbf{C}\,\boldsymbol{\varepsilon}^h$

3-node inverse shell element

First-Order Shear Deformation Theory: Flat inverse-shell element

- Kinematic assumptions account for deformations due to
  - Membrane
  - Bending
  - Transverse shear

$$u_x(\mathbf{x},t) = u + z\,\theta_y$$
$$u_y(\mathbf{x},t) = v + z\,\theta_x$$
$$u_z(\mathbf{x},t) = w$$

$$\mathbf{x} \equiv (x,\, y,\, z)$$
$$z \in [-h,\, h]$$

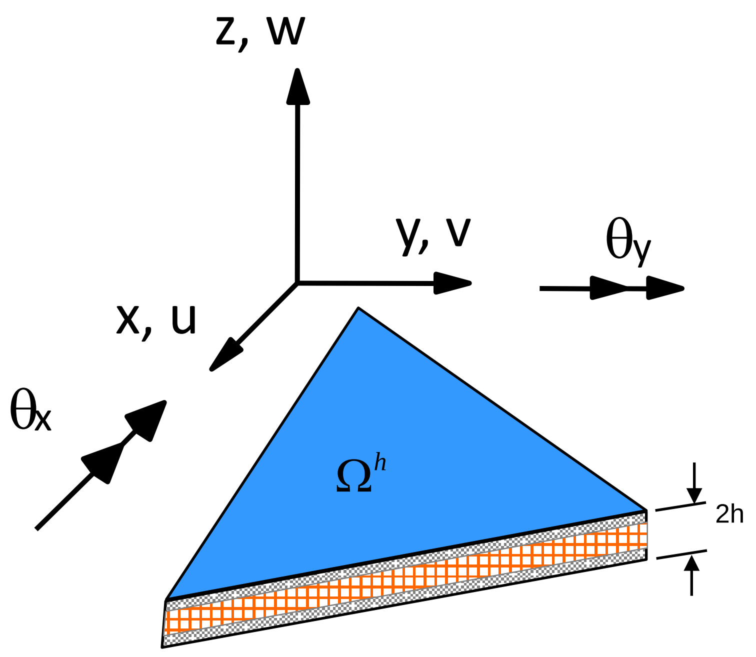

Experimental in-situ strains

In-situ surface strains

top rosette

$$\begin{Bmatrix} \varepsilon_{xx}^{+} \\ \varepsilon_{yy}^{+} \\ \gamma_{xy}^{+} \end{Bmatrix}$$

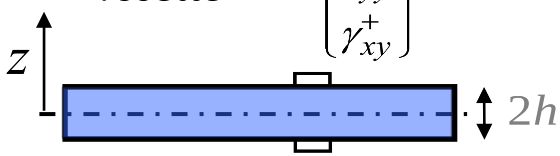

bottom rosette

$$\begin{Bmatrix} \varepsilon_{xx}^{-} \\ \varepsilon_{yy}^{-} \\ \gamma_{xy}^{-} \end{Bmatrix}$$

Experimental strains via FSDT formalism

$$\begin{Bmatrix} \varepsilon_{xx} \\ \varepsilon_{yy} \\ \gamma_{xy} \end{Bmatrix}^{\varepsilon} \equiv \begin{Bmatrix} \varepsilon_{1} \\ \varepsilon_{2} \\ \varepsilon_{3} \end{Bmatrix}^{\varepsilon} + z \begin{Bmatrix} \varepsilon_{4} \\ \varepsilon_{5} \\ \varepsilon_{6} \end{Bmatrix}^{\varepsilon}$$

Evaluate at $x_i; z = \pm h$

$$\mathbf{e}_i^{\varepsilon} \equiv \begin{Bmatrix} \varepsilon_{1} \\ \varepsilon_{2} \\ \varepsilon_{3} \end{Bmatrix}^{\varepsilon} = \frac{1}{2}\left(\begin{Bmatrix} \varepsilon_{xx}^{+} \\ \varepsilon_{yy}^{+} \\ \gamma_{xy}^{+} \end{Bmatrix} + \begin{Bmatrix} \varepsilon_{xx}^{-} \\ \varepsilon_{yy}^{-} \\ \gamma_{xy}^{-} \end{Bmatrix} \right) \qquad \mathbf{k}_i^{\varepsilon} \equiv \begin{Bmatrix} \varepsilon_{4} \\ \varepsilon_{5} \\ \varepsilon_{6} \end{Bmatrix}^{\varepsilon} = \frac{1}{2h}\left(\begin{Bmatrix} \varepsilon_{xx}^{+} \\ \varepsilon_{yy}^{+} \\ \gamma_{xy}^{+} \end{Bmatrix} - \begin{Bmatrix} \varepsilon_{xx}^{-} \\ \varepsilon_{yy}^{-} \\ \gamma_{xy}^{-} \end{Bmatrix} \right)$$

Full-Field Reconstruction using iFEM

- **Least-Squares variational formulation**
  - Plate formulation based on first-order shear deformation theory
    - Strain compatibility equations fulfilled
    - Strains treated as tensor quantities
    - No dependency on material, inertial or damping properties
  - Efficient elements for
    - Beams and frames
    - Plates and shells
  - Application to metal, multilayer composite, and sandwich structures

$$\Phi_e^p(\mathbf{u}^h) = p_1 \|\Delta\mathbf{e}\|^2 + p_2 \|\Delta\mathbf{k}\|^2 + p_3 \|\Delta\mathbf{g}\|^2$$

p_i : Positive valued weighting constants – put different importance on the satisfaction of the individual strain components and their adherence to the measured data

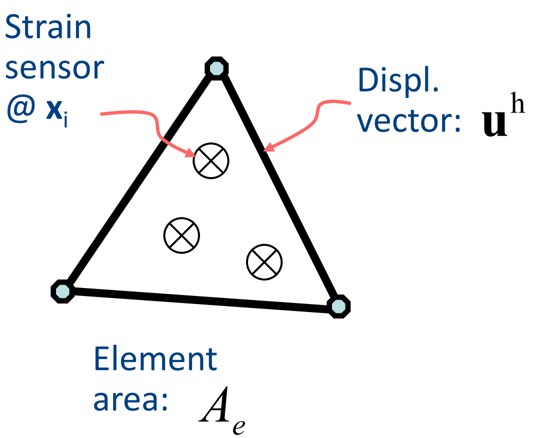

Discretization using iMIN3 elements

- Variational principle

$$\min : \sum_{e=1}^{N} \Phi_e^{\lambda}(\mathbf{u}^h) = 0$$

- Linear Eqs

$$\mathbf{A}\,\mathbf{d} = \mathbf{b}$$

- Efficient solution

$$\mathbf{d} = \mathbf{A}^{-1}\mathbf{b}$$

$\mathbf{A}(\mathbf{x}_i)$ symmetric, positive definite matrix (B.C.'s imposed)

$\mathbf{d}$ Nodal displacement vector

$\mathbf{b}$ r.h.s. vector, function of measured strain values

Coarse discretization sufficient
(more efficient than direct FEM)

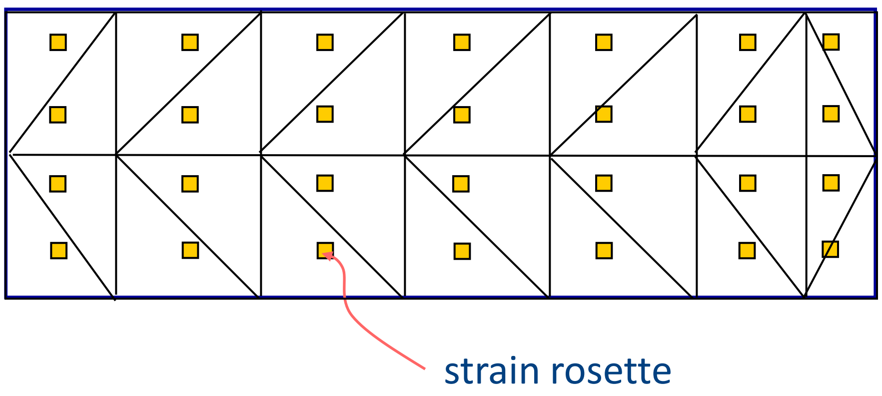

Attributes of Inverse FEM

- **Theory**
  - Strain-displacement relations fulfilled
  - Least-squares compatibility with measured strain data
  - Integrability conditions fulfilled
  - Independent of material properties
  - Stable solutions under small changes in input strain data (random error in measured strain data)
  - Geometrically linear and nonlinear (co-rotational formulation) response
  - Dynamic regime
- **Computational efficiency, architecture and modeling**
  - Architecture as in standard FEM (e.g., user routine in ABAQUS)
  - Superior accuracy on coarse meshes (advantage of integration)
  - Beam, frame, plate, shell and built-up structures
  - Thin and moderately thick regime
  - Low and higher-order elements
  - Use of partial strain data (over part of structure, or incomplete strain tensor data)
- **Studies performed**
  - Beam, frame, plate, and built-up shell structures
  - Experimental studies using FBG strains and strain rosettes
  - Transient dynamic response and strain data

iFEM applied to Plate Bending

- Strain rosette data

- FBG sensors

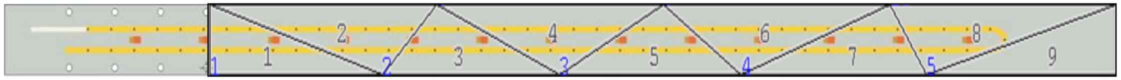

- Incomplete strain data

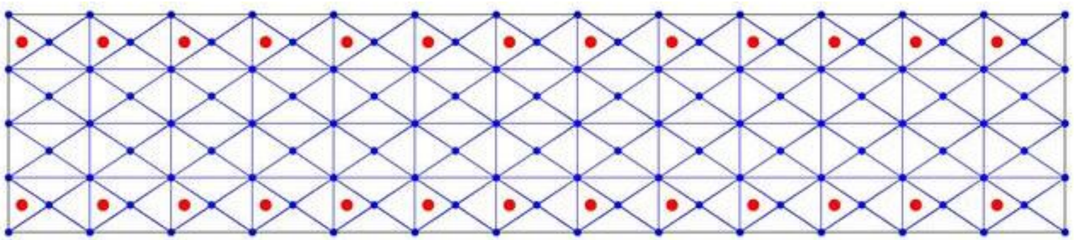

Cantilevered Plate: iFEM using experimental strains

- Aluminum 2024-T3 alloy
  - Elastic modulus: 10.6 Msi
  - Poisson's ratio: 1/3
  - Thickness: 1/8 in
- Weight loaded at (9 in,1.5 in)
  - P = 5.784 lb (2623 g)

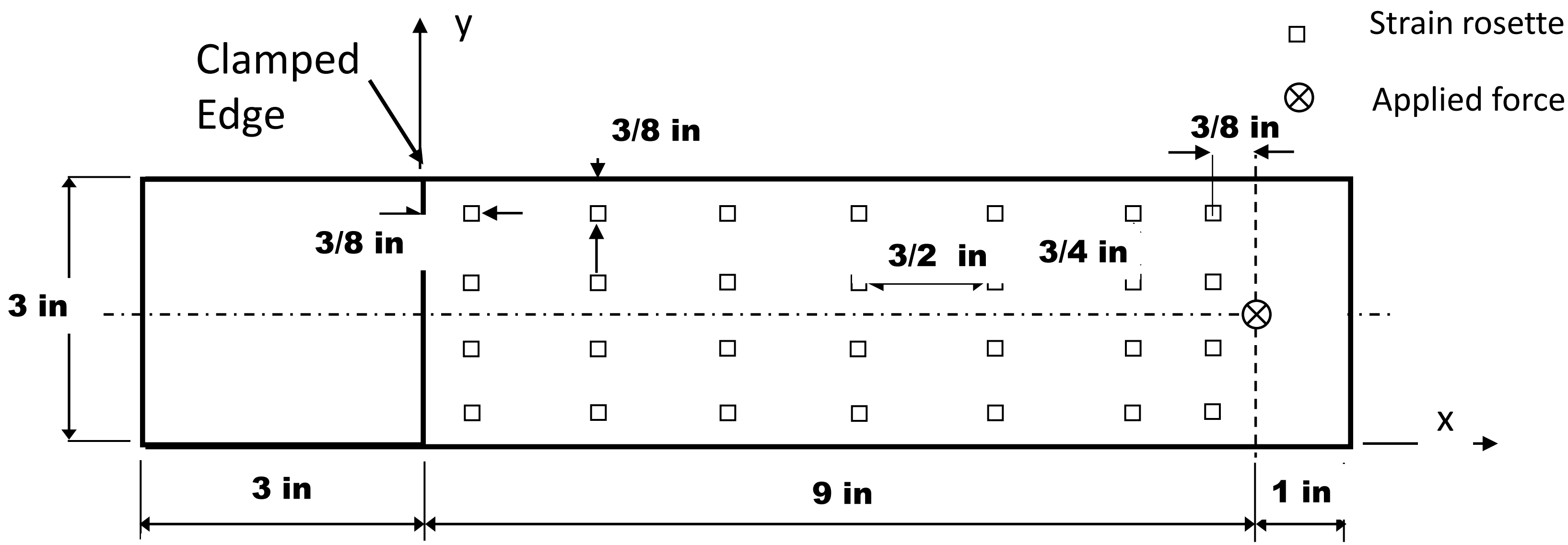

* A. Tessler & J. Spangler. EWSHM (2004); P. Bogert et al., AIAA (2003)

Deflection comparison

Measured deflection,
W = 6.81 mm,
at (214.3 mm, 38.1 mm)

FEM (ABAQUS)

Clamped edge

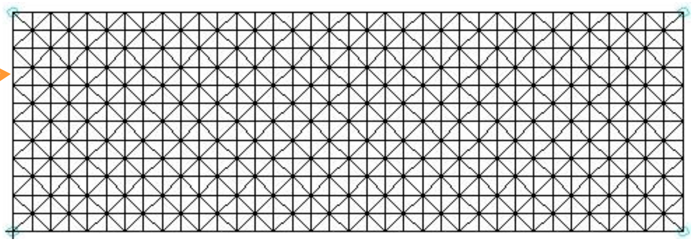

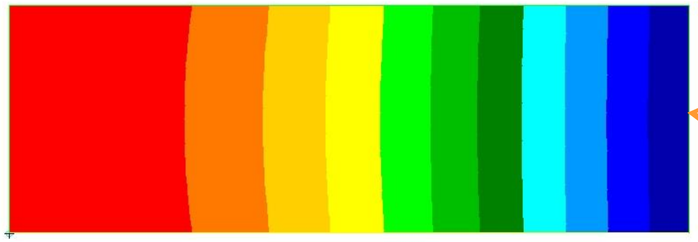

Max. deflection
W = 6.855 mm

Rossette strains

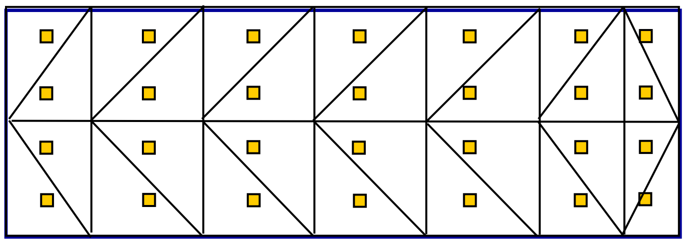

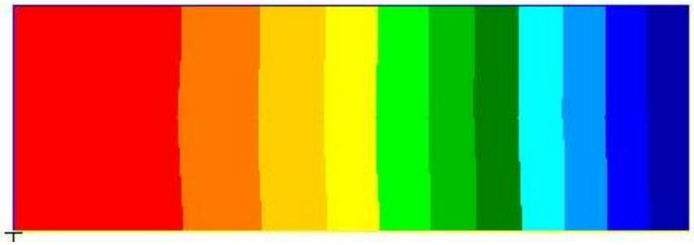

Max. deflection
W = 6.860 mm

W (in)

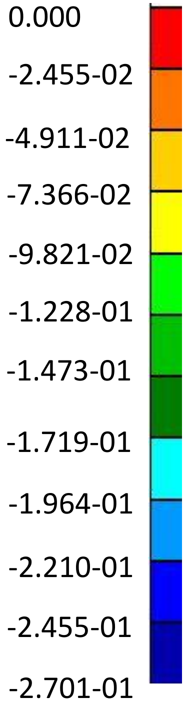

Slender Beam Experiment using FOSS/iFEM*

Beam sensor layout and iFEM mesh

Cantilever beam instrumented with FOSS fiber. Deflection predicted from strain measurements via Inverse FEM.

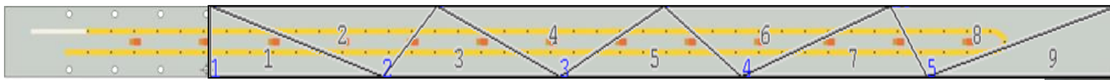

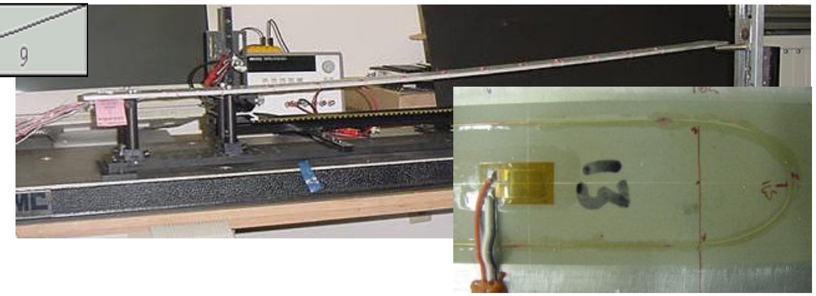

Measured and computed strain data

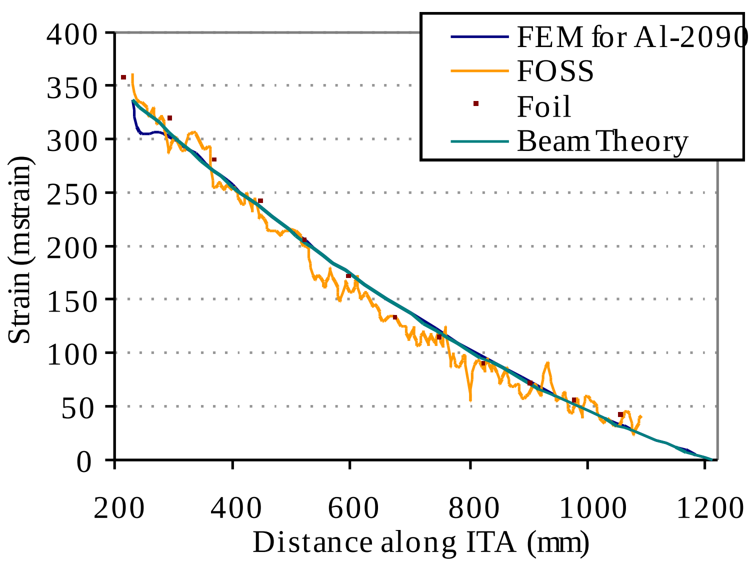

Excellent correlation of deflection

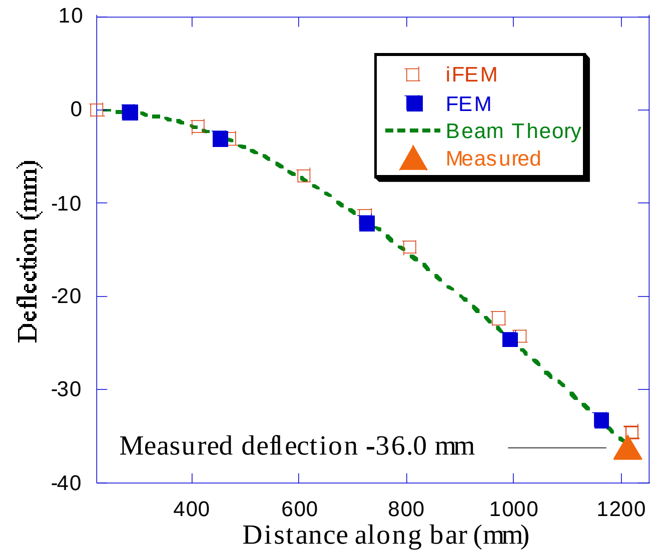

* S. Vazquez et al., NASA-TM (2005)

Cantilevered AL Plate in Bending under Uniform Load: Application of iFEM with Incomplete Strain Data

Impact:

The iFEM is well-suited for real-time monitoring of the aircraft structural response and integrity when used in conjunction with advanced strain-measurement systems based on Fiber-Optic Bragg Grading strain sensors.

Strain rosettes distributed along edges of plate

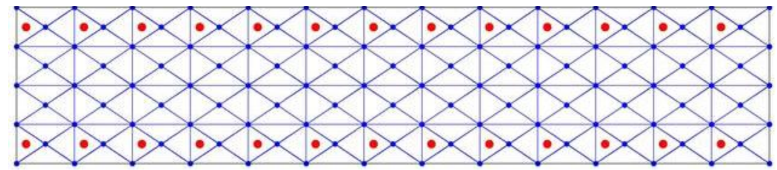

Predicted deflection error < 1.5%

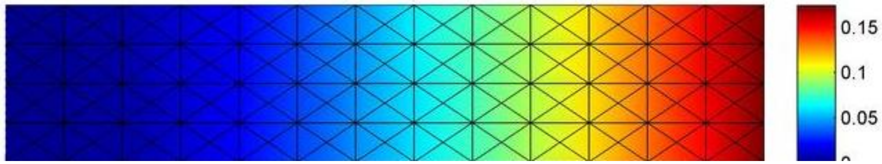

Predicts an accurate full-field deformation with a maximum deflection error of less than 1.5%. Only strain rosette measurements along panel edges are used in the analysis.

$$\Phi_e^p(\mathbf{u}^h) = p_1 \left\|\Delta\mathbf{e}\right\|^2 + p_2 \left\|\Delta\mathbf{k}\right\|^2 + p_3 \left\|\Delta\mathbf{g}\right\|^2$$

$p_i \ (i = 1,2,3):$ weighting constants are set small in elements that do not have strain data

3-D Inverse Frame Finite Element Formulation*

* Collaboration with Politecnico di Torino

Power systems

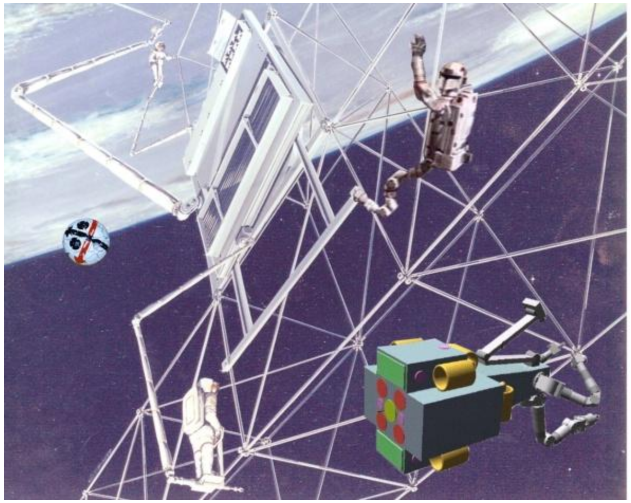

Transfer vehicles

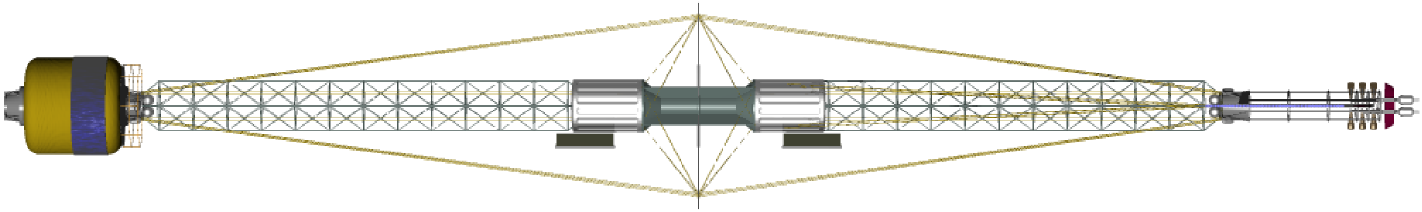

3-D Frame iFEM Formulation

Kinematic assumptions

$$\begin{cases} u_x(x,y,z) \equiv u(x) + z\theta_y(x) - y\theta_z(x) \\ u_y(x,y,z) \equiv v(x) - z\theta_x(x) \\ u_z(x,y,z) \equiv w(x) + y\theta_x(x) \end{cases}$$

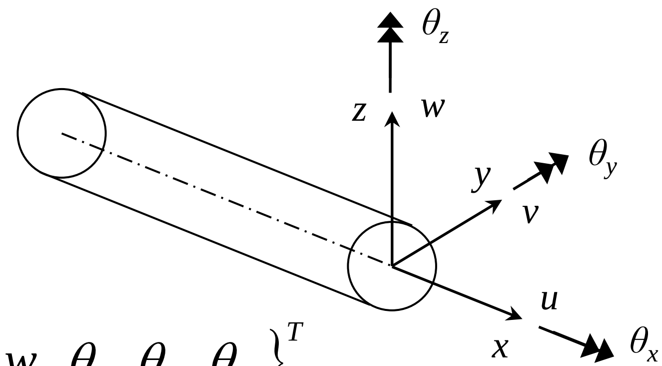

$$\mathbf{q} = \{u,\ v,\ w,\ \theta_x,\ \theta_y,\ \theta_z\}^T$$

- Strains

$$\begin{cases} \varepsilon_x = u_{,x} + z\theta_{y,x} - y\theta_{z,x} \\ \varepsilon_y = 0 \\ \varepsilon_z = 0 \\ \gamma_{xz} = (\theta_y + w_{,x}) + y\theta_{x,x} \\ \gamma_{yz} = 0 \\ \gamma_{xy} = (-\theta_z + v_{,x}) - z\theta_{x,x} \end{cases} \Rightarrow \begin{cases} \varepsilon_x = \varepsilon_{x0} + z\kappa_{y0} + y\kappa_{z0} \\ \gamma_{xz} = \gamma_{z0} + y\alpha_0 \\ \gamma_{xy} = \gamma_{y0} - z\alpha_0 \end{cases}$$

Strain measures

$$\mathbf{e}(\mathbf{q}) = \begin{Bmatrix} \varepsilon_{x0} \\ \kappa_{y0} \\ \kappa_{z0} \\ \gamma_{z0} \\ \gamma_{y0} \\ \alpha_0 \end{Bmatrix} \equiv \begin{Bmatrix} u_{,x} \\ \theta_{y,x} \\ -\theta_{z,x} \\ \theta_y + w_{,x} \\ -\theta_z + v_{,x} \\ \theta_{x,x} \end{Bmatrix}$$

Numerical assessment

- Frame structure (thin-wall cross-section)

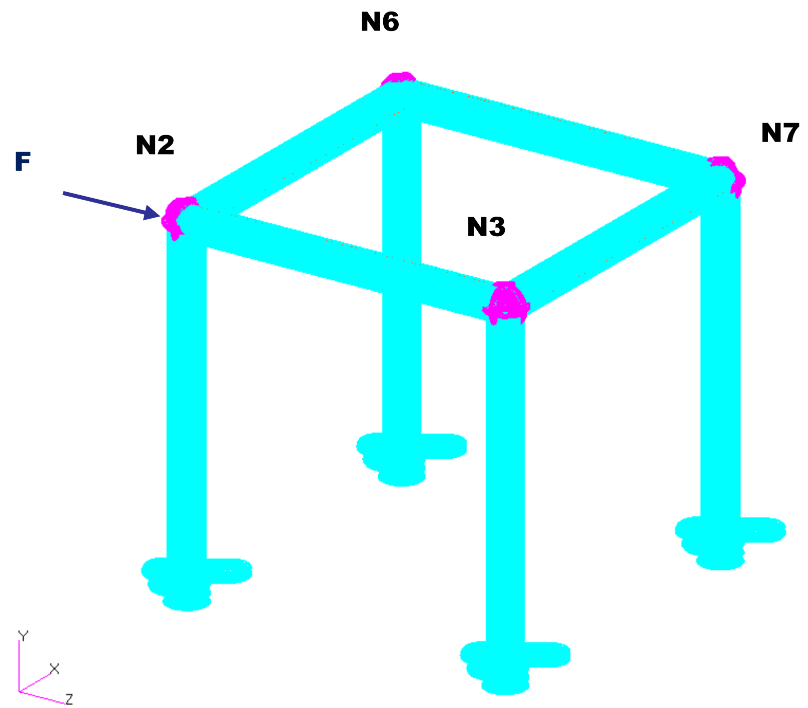

dof	iFEM/NASTRAN
u_2	1.008
v_2	1.002
w_2	1.002
θ_{x2}	1.003
θ_{y2}	1.007
θ_{z2}	1.010
u_3	1.007
v_3	1.002
w_3	1.002
θ_{x3}	1.003
θ_{y3}	1.007
θ_{z3}	1.010
u_6	1.008
v_6	1.001
w_6	0.996
θ_{x6}	0.995
θ_{y6}	1.007
θ_{z6}	1.010
u_7	1.007
v_7	1.002
w_7	0.996
θ_{x7}	0.995
θ_{y7}	1.007
θ_{z7}	1.009

- Forward and Inverse FEM model data

Element type	NASTRAN (QUAD 4)	Inverse beam FE
No. of nodes	3.29×10^5	8 (48 dofs)
No. of elem.	3.28×10^5	8

Transient response of damped cantilever beam: iFEM solution vs. high-fidelity NASTRAN model

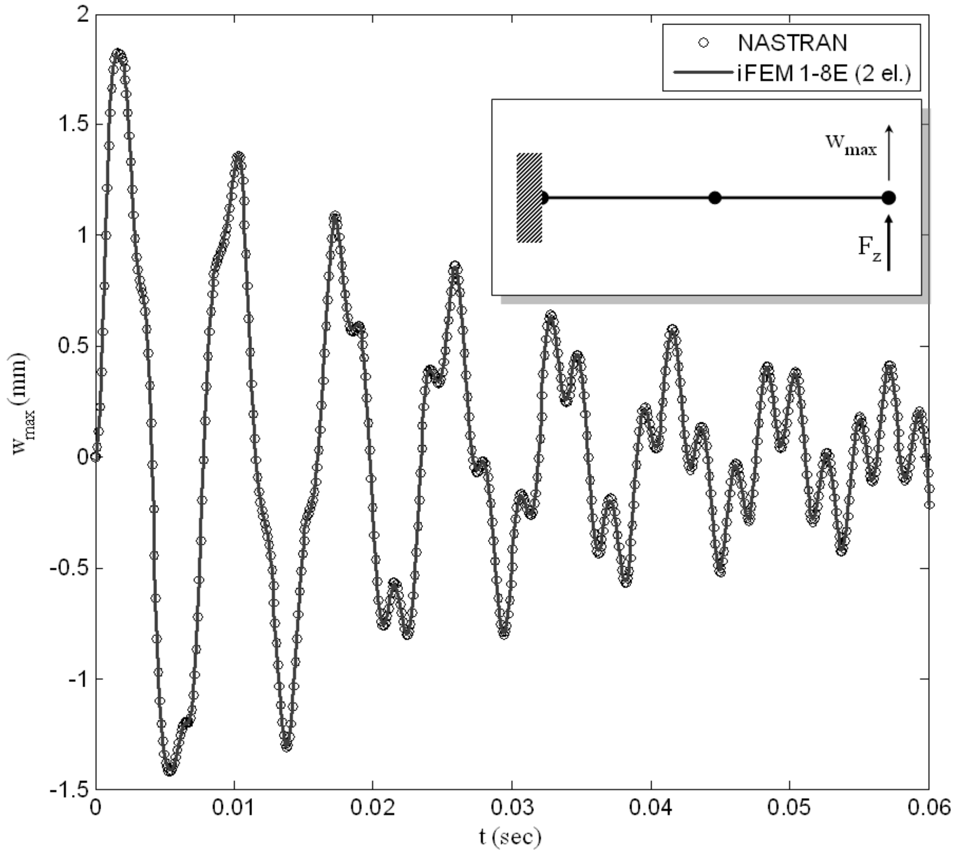

Tip beam deflection w_{max} loaded by a transverse concentrated force F_z at f_0=1,400 Hz

iFEM based on Refined Zigzag Theory for Multilayered Composite and Sandwich Structures

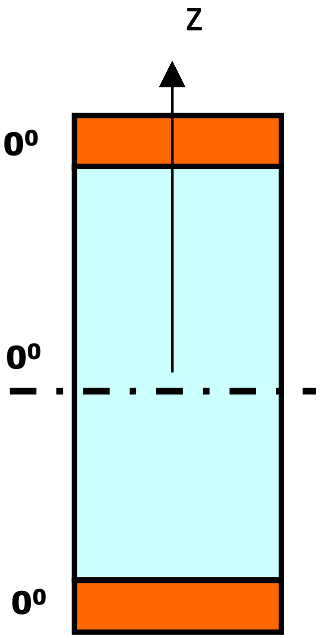

Zigzag kinematics

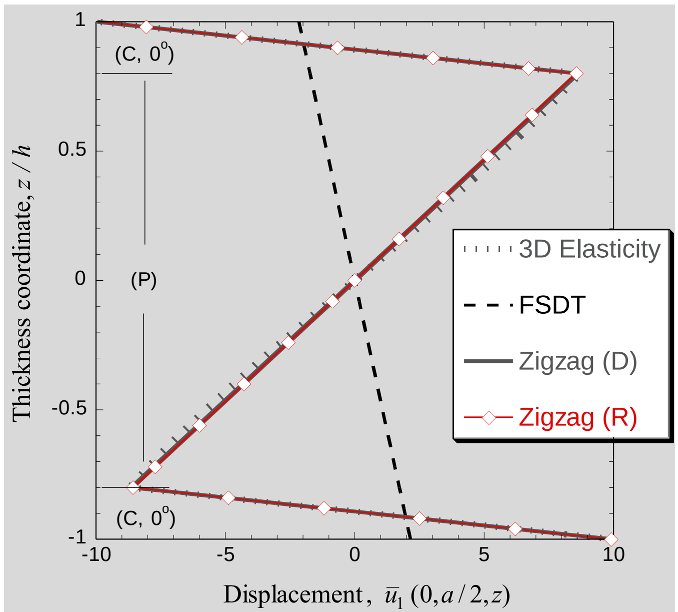

Airbus AA587

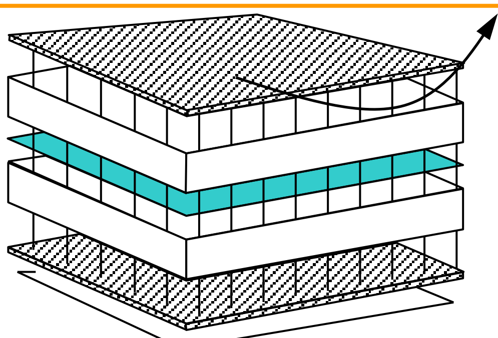

Multifunctional Sandwich Panel

- Radiation shield
- Damage tolerant
- Thermal protection

Summary

- On-board structural integrity of nextgen aircraft, spacecraft, large space structures, and habitation structures
  - Safe, reliable, and affordable technologies
- Inverse FEM algorithms using FBG strain measurements
  - Real-time efficiency, robustness, superior accuracy
  - Large-scale, full-field applications
- Inverse FEM theory
  - Strain-displacement relations & integrability conditions fulfilled
  - Independent of material properties
  - Solutions stable under small changes in input data
  - Linear and nonlinear response

Summary (cont'd)

- Inverse FEM's architecture/modeling
  - Architecture as in standard FEM (user routine in ABAQUS)
  - Superior accuracy on coarse meshes
  - Frames, plates/shell and built-up structures
  - Thin and moderately thick regime
  - Low and higher-order elements
- Inverse FEM applications
  - Computational studies: frame, plate and built-up shell structures
  - Experimental studies: FBG strains and strain rosettes
  - Dynamic strain data
  - Zigzag theory for composites

Collaborations & Interactions

- Lockheed Martin Co (J. Spangler)
- NASA LaRC (S. Vazquez, C. Quach, E. Cooper, and J. Moore)
- University of Hawaii (Prof. R. Riggs)
- Politecnico di Torino (Profs. Di Sciuva and Gherlone)

Ikhana fiber optic wing shape sensor team: clockwise from left, Anthony "Nino" Piazza, Allen Parker, William Ko and Lance Richards.

NASA Dryden Flight Research Center Photo Collection
http://www.dfrc.nasa.gov/Gallery/Photo/index.html
NASA Photo: ED08-0109-08 Date: May 1, 2008 Photo By: Tom Tschida

Ikhana fiber optic wing shape sensor team: clockwise from left, Anthony "Nino" Piazza, Allen Parker, William Ko and Lance Richards.

NASA Dryden Flight Research Center Photo Collection
http://www.dfrc.nasa.gov/Gallery/Photo/index.html
NASA Photo: ED07-0038-052 Date: March 5, 2007 Photo By: Tony Landis

Figure 1. Ikhana unmanned science and technology development aircraft.

Publications

- Tessler, A. and Spangler, J. L.: A Variational Principle for Reconstruction of Elastic Deformations in Shear Deformable Plates and Shells. NASA/TM-2003-212445 (2003).
- Tessler, A. and Spangler, J. L.: Inverse FEM for Full-Field Reconstruction of Elastic Deformations in Shear Deformable Plates and Shells. NASA/TM-2004-090744 (2004).
- Prosser*, W. H., Allison, S. G., Woodard, S. E., Wincheski, R. A.; Cooper, E. G.; Price, D. C., Hedley, M., Prokopenko, M., Scott, D. A., Tessler, A., and Spangler, J. L.: Structural Health Management for Future Aerospace Vehicles. Proceedings of 2nd Australasian Workshop on Structural Health Monitoring (2004).
- Vazquez, S. L., Tessler, A., Quach, C. C., Cooper, E. G., Parks, J., and Spangler, J. L.: Structural Health Monitor Using High-density Fiber Optic Networks and Inverse Finite Element Method. Air Force Research Laboratory Integrated Systems Health Management Conference, August 17-19, 2004, Dayton, Ohio; Also NASA/TM-2005-213761 (2005).
- Tessler, A. and Spangler, J. L.: A Least-Squares Variational Method for Full-Field Reconstruction of Elastic Deformations in Shear-Deformable Plates and Shells. Computer. Methods Appl. Mech. Engrg. Vol. 194, 327-329 (2005).
- Gherlone, M., Mattone, M., Surace, C., Tassotti*, A., and Tessler, A.: Novel Vibration-based Methods for Detecting Delamination Damage in Composite Plate and Shell Laminates. Key Engineering Materials, Vols. 293-294, 289-296 (2005).
- Tessler A.: Structural analysis methods for structural health management of future aerospace vehicles. NASA/TM-2007-214871 (2007).
- Gherlone M. Beam inverse finite element formulation. Politecnico di Torino, Oct. 2008.
- Cerracchio P., Gherlone M., Mattone M., Di Sciuva M., and Tessler A.: Inverse finite element method for three-dimensional frame structures. NASA/TP-2011, 2011.